Pressure-Induced Isostructural Antiferromagnetic-Ferromagnetic Transition in an Organic Electride

Stephen G. Dale,[*,†] A. Otero-de-la-Roza,[*,‡] and Erin R. Johnson[*,†]

†*Department of Chemistry, Dalhousie University, 6274 Coburg Rd, P.O.Box 15000 B3H 4R2, Halifax, Nova Scotia, Canada*

‡*Department of Chemistry, University of British Columbia, Okanagan, 3247 University Way, Kelowna, British Columbia, Canada V1V 1V7.*

E-mail: stephen.dale@dal.ca; aoterodelaroza@gmail.com; erin.johnson@dal.ca

Abstract

Electrides are ionic solids in which cavity-trapped electrons act as anions. These materials have a number of unusual magnetic and electronic properties that originate from the free electrons localised in the crystal voids. Antiferromagnetic behaviour has previously been observed in organic electride crystals, while recently it has been shown that two-dimensional electrides show strongly anisotropic electrical conductivity and weak itinerant ferromagnetism. In this work, we study the behaviour of the simplest organic electride ($Cs^+(15\text{-crown-}5)_2e^-$) under pressure using dispersion-corrected density-functional theory. We predict that this electride undergoes an antiferromagnetic to ferromagnetic isostructural transition in the 0.5 to 1.0 GPa range. The electride character of the material is preserved through the transition, which originates exclusively from the spin coupling of the electrons trapped in the crystal voids. The

pressure required for the magnetic transition is easily accessible using modern experimental techniques, which opens the door to potential magnetoelectric applications for the electride materials.

Introduction

Electrides[1–3] are ionic solids in which anions are stoichiometrically replaced with electrons localised within crystal voids. These electrons originate from the ionization of nearby moieties with relatively low ionization potentials, which, after losing their valence electron, function as the cations in the ionic electride material. Due to their unique electronic structure, electrides possess unusual electronic, optical, and magnetic properties,[3–5] which makes their study valuable for their potential usefulness in electronic devices.[6,7]

Electrides are typically classified by the topology of their void electrons in real space. Free electrons can be localised in disconnected crystal cavities (zero-dimensional electrides, 0D), delocalised over channels (one-dimensional, 1D), etc. The topology of the cavities where the electrons are hosted directly affects the macroscopic properties of electride crystals, particularly their electric conductance and magnetic properties.[8–10] Zero- and one-dimensional organic electrides composed of alkali and alkaline-earth metal complexes with electron-donating ligands (crown ethers, nitrogen cryptands) were described and characterised long ago.[2–4]

Experimental challenges in their synthesis, primarily their thermal and atmospheric instability, have hindered the investigation of electrides.[3] The $12CaO{\cdot}7Al_2O_3$ inorganic electride, synthesised in 2003 by Matsuishi et al.,[11] is remarkable not only in that it has a radically different structure from previous electrides—a microporous solid with excess valence electrons—but also in that it is stable at room temperature.[3,11,12] In a recent article, Lee et al.[13] reported the synthesis of Ca_2N, the first instance of a 2D electride, in which free electrons are delocalised over an interstitial layer. Thanks to these efforts, the study of electrides and their potential applications has experienced a resurgence in the literature.[14,15] To date, five inorganic electrides have been synthesised and characterised experimentally,[11,13,15–17] and numerous computational and database explorations have been conducted in search for new stable electrides.[18–22]

Due to the complexity of their experimental study, theoretical modeling is often employed to characterize new electride materials. Electrides, particularly one- and two-dimensional

have been shown to present highly anisotropic band structures[18,19] and magnetic properties.[20,23] Carbide electride materials, and in particular the recently synthesised Y_2C compound,[7,16,20,23] have become very popular due to their unusual magnetic properties. In particular, strongly anisotropic electrical conductivity and magnetization and, in some cases, weak itinerant ferromagnetism caused by the mobility of the interstitial electrons,[16,23] as well as topological behaviour.[24] It has been recently predicted that pressure-induced phase transitions in Y_2C quench its electride character.[25]

In 2014, we presented a systematic examination of the seven organic and one inorganic electride crystals known at the time using dispersion-corrected density-functional theory.[26] We showed that the experimentally known insulating character, and the antiferromagnetic (AFM) ordering[1] can be reproduced using density functional theory[27] in 0D and 1D electrides. In all cases, the AFM magnetic ordering arises from the distant exchange interactions between the spins of electrons trapped in separate cavities. Dye *et al.*[8] and Ryanbinkin and Staroverov[10] found strong correlations between the magnetic coupling constant (J) and the cross-sectional area of both the interstitial voids and channels through which they are connected. This relationship suggests that it is possible to tune the magnetic properties of electride materials through external perturbations like applied pressure.

In this study, we use dispersion-corrected density-functional theory calculations to model the behaviour of the simplest organic electride, $Cs^+(15\text{-crown-}5)_2e^-$ under pressure. Experimentally, it is known that this electride has antiferromagnetic ordering at zero pressure.[1] We show that, under applied hydrostatic pressure, $Cs^+(15\text{-crown-}5)_2e^-$ displays unusual magnetic behaviour: an antiferromagnetic to ferromagnetic (FM) isostructural transition, which is not predicted by previous studies based on simple magnetic models. The electride character of the material is preserved through the magnetic transition, as well as its insulating character. Pressure-induced (or strain-induced) magnetic transitions are essential in the design of spintronic and other next-generation electronic devices. A recent example is the work of Li et al., who predicted a strain-induced FM to AFM magnetic transition in a

doped silicene monolayer.[28]

Computational methods

The effect of hydrostatic pressure on the magnetic properties of $Cs^+(15\text{-crown-}5)_2e^-$ (71 atoms in the primitive unit cell) is examined using the planewaves/pseudopotentials (PW/PS) approach and the Projected Augmented Wave (PAW) formalism under periodic boundary conditions.[29] All calculations were conducted using the Quantum ESPRESSO[30] package with 50 Ry cut-off energy, a 4×4×4 $\boldsymbol{k}$-points mesh, cold smearing[31] with a smearing temperature of 0.01 Ry, and spin polarisation. Pressure was applied using the calculated stress tensor.[32] Two different density functionals, PBE[33] and B86bPBE[34] were utilised, and the exchange-hole dipole dispersion moment model (XDM)[35–38] was used to account for dispersion effects. We explored a pressure range from −0.5 GPa to 3 GPa, which results in a 26% decrease in volume of the unit cell at the highest applied pressure. Negative pressures are included in order to model the effect of thermal expansion at zero pressure.[37] The crystal geometry was fully relaxed at each applied pressure.

The choice of magnetic state was made by setting the initial magnetization in the self-consistent field (SCF) calculation. In the case of the ferromagnetic ordering, the spin density of the eight hydrogen atoms closest to the crystal void were set to contribute only α density.[27] As the unit cell of $Cs^+(15\text{-crown-}5)_2e^-$ only contains one crystal void, the only possible magnetic solution for a calculation using a single unit cell is ferromagnetic. To obtain the antiferromagnetic solution, the fully relaxed $Cs^+(15\text{-crown-}5)_2e^-$ unit cell was doubled in each direction to generate a $2 \times 2 \times 2$ supercell with 8 crystal voids. Single-point calculations were carried out on these supercells using XDM, cut-off energy, and smearing-temperature parameters identical to the single-cell calculations and a single $\boldsymbol{k}$-point at Γ. The spin bias applied to each hydrogen atom described above was either preserved (ferromagnetic) or alternated between neighbouring unit cells (antiferromagnetic).

Since the equations of state of both magnetic orderings are virtually identical, the relative stability of the AFM and FM states as a function of pressure can be evaluated using the calculated magnetic coupling constant, as in our previous work:[27]

$$J = 1/2(E_{\mathrm{AFM}} - E_{\mathrm{FM}}) \tag{1}$$

Note that the coupling constants for electrides are typically reported as $-J/k_B$ as electrides all posses negative coupling constants (J) reflective of their antiferromagnetic character. In this work, the opposite convention is used: Antiferromagnetic (ferromagnetic) orderings correspond to a negative (positive) J.

To monitor the volume of the interstitial crystal voids we use the pro-crystal void volume, which is calculated as the volume of the region where the pro-crystal density (the sum of atomic densities) is lower than 0.001 a.u. We use Bader charges[39] to evaluate the electron population inside the crystal voids since, as we shall see, the localised electron in an electride is always associated to a non-nuclear maximum (NNM) of the electron density.[26,27,40,41] The integration of the Bader basins is performed using the critic2 program[42,43] with the Yu-Trinkle algorithm.[44]

Results and Discussion

Figure 1 shows the evolution of J with pressure. At low pressure, $J < 0$ and the AFM ordering is more stable, which is consistent with experimental observations.[9] The PBE-XDM coupling constant at zero pressure is -2.7 K, in excellent agreement with the experimental value (-3 K).[9] However, this agreement may be coincidental as our calculations do not account for vibrational effects, which would shift both curves in Figure 1 to higher pressures. For instance, the calculated equilibrium void volume is 90 Å^3, considerably smaller than the experimental result (142 Å^3, see the Supplementary Information for details on the calculation of the void volumes). The -0.5 GPa crystal geometry is actually much closer to

Figure 1: Pressure dependence of the magnetic coupling constant (J/k_B) in $Cs^+(15\text{-crown-}5)_2e^-$ calculated using the B86bPBE-XDM (black) and PBE-XDM (red) functionals. The horizontal blue line at −3 K gives the experimental value of the coupling constant[9] at the crystal's equilibrium geometry.

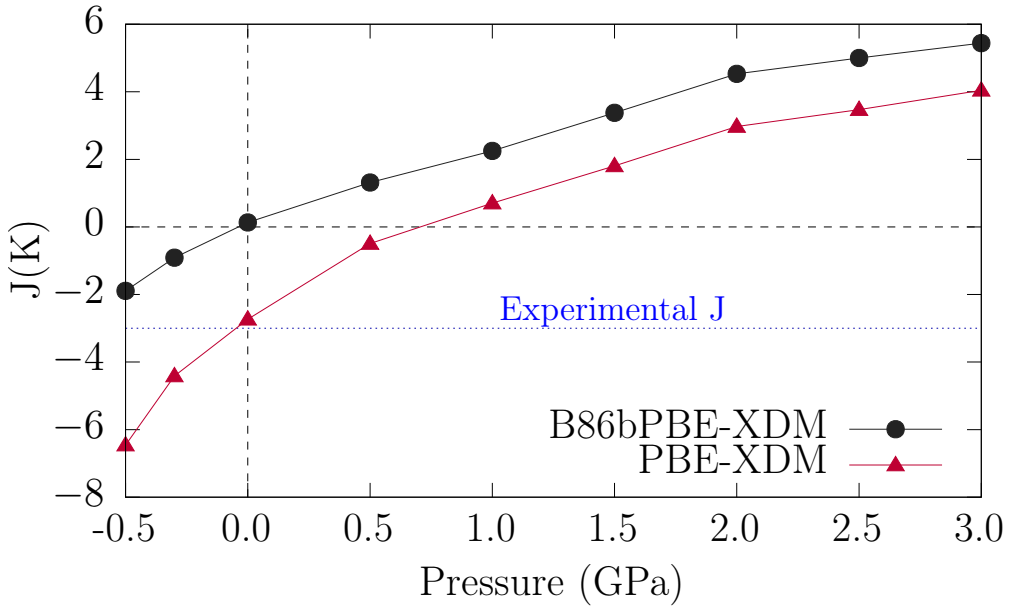

the experimental value, with crystal void volumes slightly smaller than 140 Å^3. Assuming a thermal pressure[37] of −0.5 GPa, the B86bPBE-XDM result both matches the experimental volume and gives a reasonable approximation to the observed magnetic coupling constant (−1.9 K).

Figure 1 shows that both functionals predict an isostructural pressure-induced AFM to FM transition in this electride in the 0.5–1.0 GPa range. This magnetic transition is unexpected because it is not predicted by previous studies based on model spin Hamiltonians[10] and previous assumptions in the literature.[4] It is also unusual because the transition is isostructural and involves only the electrons in the crystal voids, without mediation from the molecular moieties.

To study the nature of this transition in more detail, we conducted an analysis of the electron densities and spin densities as well as the band structure of both magnetic orderings. Figure 2 shows the band structure for the AFM (0 GPa) and FM (3 GPa) phases calculated

Figure 2: Band structure of the antiferromagnetic (left) and ferromagnetic (right) states of $Cs^+(15\text{-crown-}5)_2e^-$ at 0 and 3 GPa, respectively, using the PBE+XDM functional. The antiferromagnetic band structures were calculated using a $2 \times 2 \times 2$ supercell and hence show 8 "electride bands" near the Fermi level. The α and β bands in the antiferromagnetic case are essentially coincident, and only one set of bands is shown.

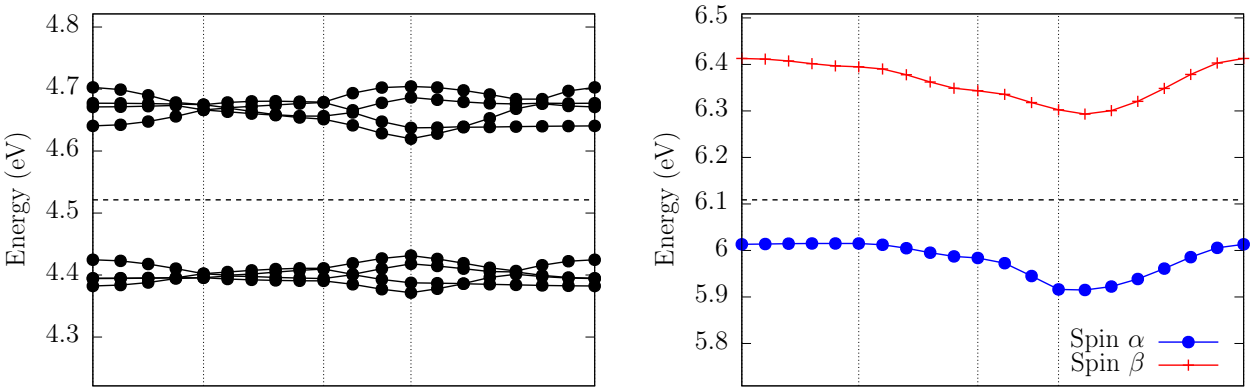

using PBE-XDM. In both cases, the electride is an insulator, in agreement with our previous results and experimental observations.[26,45] This result is remarkably different from the magnetic ordering in Y_2C and other carbides, which are predicted to present, or are on the verge of presenting, weak itinerant ferromagnetism,[46] with a heavily spin-biased density of states near the Fermi level. This itinerant ferromagnetism has also been predicted for some high pressure phases of alkali metals that also display electride behaviour.[47] In contrast, the magnetic transition in $Cs^+(15\text{-crown-}5)_2e^-$ originates purely from a spin flip of the localised electrons.

The real-space analysis of the electron and spin densities is fully consistent with the band structures shown in Figure 2. Analysis of the electron densities using the Quantum Theory of Atoms in Molecules (QTAIM)[39,43] reveals non-nuclear maxima (NNM) within the crystal voids at all pressures and in both magnetic orderings. (This is true for both functionals, but for simplicity we limit the discussion to PBE-XDM results.) Figure 3 shows a typical electride NNM in the [010] plane ($y = 0.5$ in fractional coordinates) localized in the crystal void. The electride basin, also shown in the figure, spans a significant fraction of the crystal void, although it is much smaller than the voids calculated using the promolecular density

Figure 3: Left: density contour plot in a $y = 1/2$ cross section of the unit cell intersecting the non-nuclear maximum position (in the center of the plot). Right: graphical representation of the Bader basin calculated with YT. The basin surface is coloured by density value (brighter = higher density). Both plots correspond to zero pressure, antiferromagnetic, PBE-XDM calculations.

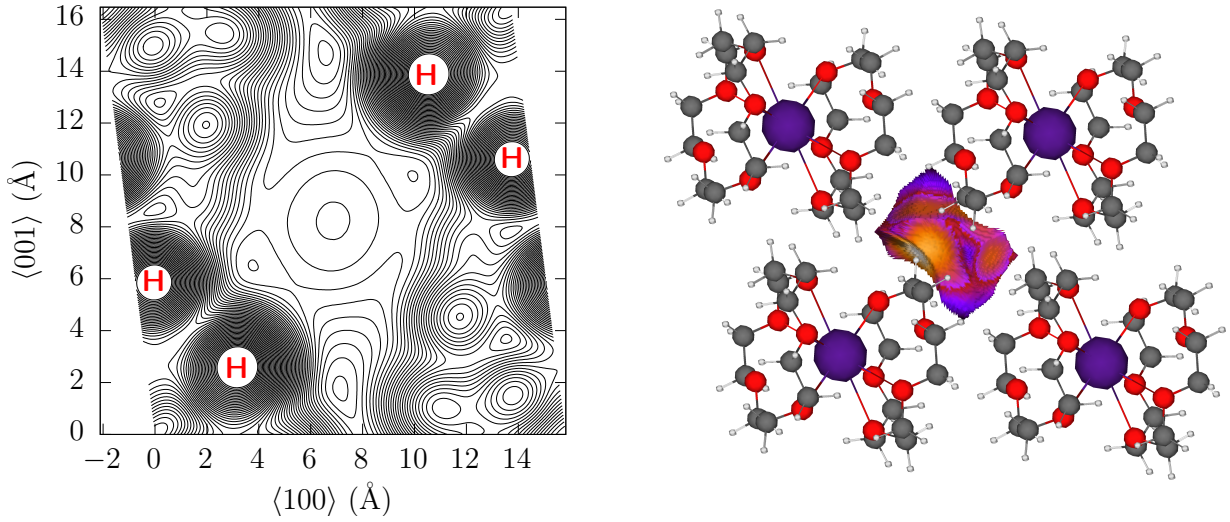

Table 1: Properties of the non-nuclear maxima (NNM) as a function of pressure (p) with both magnetic orderings using PBE-XDM. The quantities listed are: calculated magnetic coupling constant (J), void volume (V_{void}), and density (ρ_{nnm}), volume (V_{nnm}), and electron population (N_{nnm}) of the NNM. The NNM properties are obtained as an average over the eight NNM in the supercell (the variance is negligible).

			Antiferromagnetic phase			Ferromagnetic phase		
p (GPa)	J/k_B (K)	V_{void} (Å^3)	ρ_{nnm} (10^{-3} a.u.)	V_{nnm} (Å^3)	N_{nnm} (a.u.)	ρ_{nnm} (10^{-3} a.u.)	V_{nnm} (Å^3)	N_{nnm} (a.u.)
−0.5	−6.46	445.10	1.341	33.56	0.249	1.332	33.36	0.247
−0.3	−4.41	341.92	1.538	28.90	0.246	1.530	28.78	0.245
0.0	−2.73	269.75	1.750	25.50	0.247	1.744	25.41	0.245
0.5	−0.49	208.51	1.986	22.17	0.243	1.980	22.10	0.242
1.0	0.70	164.37	2.187	19.00	0.231	2.181	18.94	0.229
1.5	1.80	122.58	2.377	14.81	0.197	2.369	14.70	0.196
2.0	2.97	90.38	2.582	10.94	0.159	2.572	10.77	0.156
2.5	3.47	74.91	2.732	9.75	0.150	2.721	9.56	0.147
3.0	4.04	59.46	2.908	8.18	0.133	2.896	7.96	0.130

used in previous studies.[26]

Table 1 shows the calculated properties of the NNM as a function of pressure in both magnetic ordering using PBE-XDM. In all cases, the NNM is located at or very near the centre of the unit cell, $x = (1/2, 1/2, 1/2)$. Regardless of the magnetic ordering, the maximum interstitial charge is ca. 0.25 electrons and remains effectively constant between -0.5 and 0.5 GPa. At higher pressures, the electron population of the NNM slowly decreases as the crystal voids become smaller. At the same time, increasing pressure raises the density at the NNM position, indicating that due to the decrease in the volume available to form an electride, the unpaired electrons are being pushed back onto the molecular moieties. The NNM population is 0.13 electrons at 3 GPa. These observations are reasonable, since voids have a high local compressibility, and suggest that electride formation depends on both the available space within the electride crystal and on the relative stability of the crystal voids and the molecular moieties.[48] In all cases, the NNM only occupies a small fraction of the void volume as measured by the pro-crystal densities.

Table 1 also shows that the density at the NNM and their integrated charges and volumes are virtually identical for the FM and AFM states. This indicates that the electron population of the void is controlled by the applied pressure, and that the differences between the FM and AFM orderings cannot be explained by these data alone. This result is reasonable, since we expect the appearance and population of the NNMs is controlled by the relative electrostatic potential between the voids and the molecular moieties. Spin coupling and exchange interactions are responsible for the energy differences between the AFM and FM states, and these are typically a minor contribution to the total energy.

Figure 4 shows the spin density plots on both sides of the AFM-FM transition, at -0.5 GPa (AFM) and 3.0 GPa (FM). Table 2 shows the integrated magnetic moments in the NNM, the molecular moieties, and the cell magnetization. In agreement with the band structures and the QTAIM results, unpaired electrons are localised in the voids. In both magnetic states, there is significant magnetic moment contributions outside the NNM

Figure 4: Spin-density plots using the PBE-XDM density functional (i.e. PBE α minus β densities computed at the PBE-XDM-optimized structures) for the antiferromagnetic ground state at a pressure of -0.5 GPa (left) and the ferromagnetic ground state at a pressure of 3.0 GPa (right). The blue and red surfaces correspond to excess α and β spin densities plotted using density isovalues of ± 0.001 a.u.

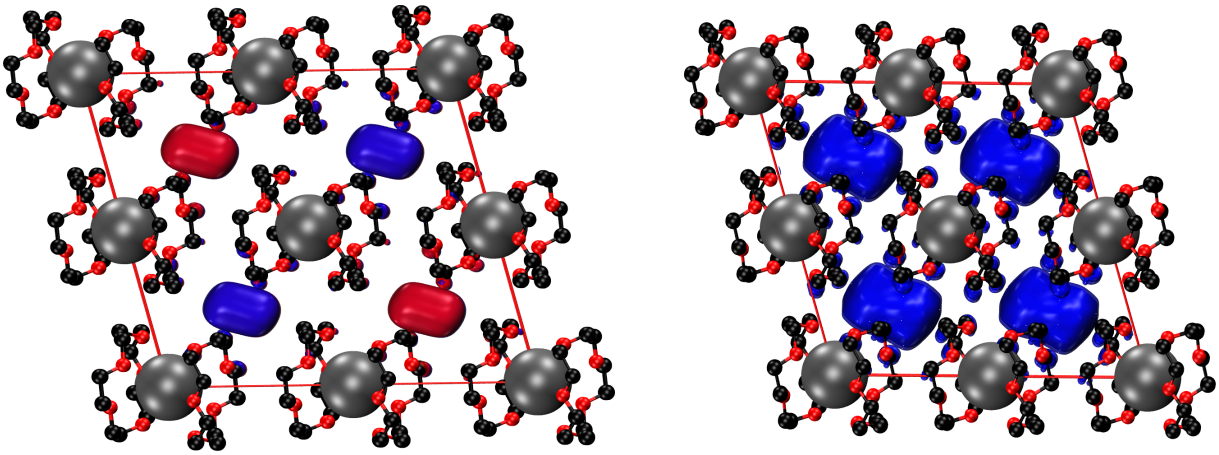

Table 2: Integrated magnetic moments (in μ_B) in the non-nuclear maxima (m_{nnm}), molecules (m_{mol}), and cell magnetization (M) as a function of pressure (p) using PBE-XDM. The calculated coupling constant (J) is also shown.

		Antiferromagnetic phase			Ferromagnetic phase		
p (GPa)	J/k_B (K)	m_{nnm}	m_{mol}	M	m_{nnm}	m_{mol}	M
-0.5	-6.46	0.220	3.752×10^{-6}	6.006×10^{-6}	0.219	0.703	7.374
-0.3	-4.41	0.220	6.433×10^{-6}	6.668×10^{-5}	0.219	0.728	7.581
0.0	-2.73	0.223	1.056×10^{-5}	1.992×10^{-4}	0.222	0.747	7.752
0.5	-0.49	0.221	3.905×10^{-6}	2.125×10^{-6}	0.220	0.764	7.874
1.0	0.70	0.210	4.696×10^{-6}	1.027×10^{-5}	0.209	0.784	7.942
1.5	1.80	0.179	1.088×10^{-5}	-2.129×10^{-4}	0.178	0.819	7.973
2.0	2.97	0.144	1.024×10^{-5}	6.439×10^{-5}	0.141	0.857	7.989
2.5	3.47	0.135	1.205×10^{-5}	-8.244×10^{-5}	0.133	0.867	7.995
3.0	4.04	0.120	5.790×10^{-6}	-3.383×10^{-5}	0.117	0.883	7.998

basin and in the atomic basins surrounding the crystal void. This is indicated by the small domains associated to the molecular hydrogen atoms in Figure 4, and in the fact that the molecular magnetic moment in the FM ordering contribute a significant amount to the cell magnetization. In the AFM case, the molecular magnetic moment is zero, but only because the same molecule is shared between an equal number of adjacent voids with opposite signs of magnetic moment. The figure shows that there a significant amount of non-zero spin density spills out of the NNM basin. Comparing the NNM populations and moments in Tables 1 and 2, we see that the crystal void is populated almost exclusively by a single electron of either spin, and that the magnetic moment is transferred to the molecular moieties under increasing pressure.

In summary, our results seem to suggest that the change in the geometry of crystal voids and channels in the crystal affects the unpaired electrons in two significant ways: the electron population of the void is reduced and, in parallel, the ferromagnetic state is stabilized. This likely originates from variations in the spin coupling and exchange interactions between localized electrons but, given the large amount of delocalisation of the interstitial electron and the complex geometry of the crystal, it is difficult to explain our results based on simple model systems.

Conclusions

We have predicted computationally that Cs^+(15-crown-5)$_2e^-$, a simple 0D organic electride, displays a pressure-induced isostructural antiferromagnetic (AFM) to ferromagnetic (FM) transition at a pressure of 0.5 to 1 GPa. Analysis of the band structure under pressure shows that the transition occurs in the presence of a non-vanishing band gap, and that the electride behaviour of the system is preserved after the change in magnetic ordering.

The electron density was studied using Bader's Quantum Theory of Atoms in Molecules (QTAIM). It was shown that non-nuclear maxima (NNM) of the electron density appear at

all pressures and in both magnetic orderings, although the electron population and volume of the NNM basin decreases with applied pressure. In addition, The integrated quantities are also essentially independent of the magnetic state. Integration of the spin density gives NNM magnetic moments that are also equal for the AFM and FM orderings in absolute value. However, there are non-negligible contributions to the overall magnetization from outside the NNM basin, with significant non-zero spin density on the hydrogen atoms surrounding the crystal voids.

Due to the complex geometry of the electride crystal and the spin interactions between unpaired electrons, it is difficult to rationalize these results in terms of simple magnetic model systems. However, our results predict yet another example of the unusual magnetic and electronic properties displayed by electrides, and highlights their potential in the design of spintronic and next-generation electronic devices.

Acknowledgements

S.G.D and E.R.J would like to thank the Natural Sciences and Engineering Research Council of Canada (NSERC) for financial support and the Multi-Environment Computer for Exploration and Discovery (MERCED), as well as Compute Canada (ACEnet and Westgrid), for computational time. S.G.D would also like to thank Dr Axel D. Becke for ongoing support.

References

(1) Dawes, S. B.; Eglin, J. L.; Moeggenborg, K. J.; Kim, J.; Dye, J. L. $Cs^+(15\text{-crown-}5)_2e^-$. A crystalline antiferromagnetic electride. *J. Am. Chem. Soc.* **1991**, *113*, 1605.

(2) Dawes, S. B.; Ellaboudy, A. S.; Dye, J. L. Cesium-133 solid-state nuclear magnetic resonance spectroscopy of alkalides and electrides. *J. Am. Chem. Soc.* **1987**, *109*, 3508–3513.

(3) Dye, J. L. Electrons as anions. *Science* **2003**, *301*, 607–608.

(4) Dye, J. L. Electrides: Ionic salts with electrons as the anions. *Science* **1990**, *247*, 663–668.

(5) Guan, S.; Huang, S. Y.; Yao, Y.; Yang, S. A. Tunable hyperbolic dispersion and negative refraction in natural electride materials. *Phys. Rev. B* **2017**, *95*, 165436.

(6) Hu, J.; Xu, B.; Yang, S. A.; Guan, S.; Ouyang, C.; Yao, Y. 2D electrides as promising anode materials for Na-ion batteries from first-principles study. *ACS Appl. Mater. Interfaces* **2015**, *7*, 24016–24022.

(7) Hou, J.; Tu, K.; Chen, Z. Two-dimensional Y_2C electride: A promising anode material for Na-Ion batteries. *J. Phys. Chem. C* **2016**, *120*, 18473–18478.

(8) Dye, J. L.; Wagner, M. J.; Overney, G.; Huang, R. H.; Nagy, T. F.; Tomanek, D. Cavities and channels in electrides. *J. Am. Chem. Soc.* **1996**, *118*, 7329–7336.

(9) Dye, J. L. Electrides: From 1D heisenberg chains to 2D pseudo-metals. *Inorg. Chem.* **1997**, *36*, 3816–3826.

(10) Ryabinkin, I. G.; Staroverov, V. N. Interelectron magnetic coupling in electrides with one-dimensional cavity-channel geometry. *Phys. Chem. Chem. Phys.* **2011**, *13*, 21615–21620.

(11) Matsuishi, S.; Toda, Y.; Miyakawa, M.; Hayashi, K.; Kamiya, T.; Hirano, M.; Tanaka, I.; Hosono, H. High-density electron anions in a nanoporous single crystal: $[Ca_{24}Al_{28}O_{64}]^{4+}(4e^-)$. *Science* **2003**, *301*, 626–629.

(12) Kim, S. W.; Hosono, H. Synthesis and properties of $12CaO{\cdot}7Al_2O_3$ electride: review of single crystal and thin film growth. *Philos. Mag.* **2012**, *92*, 2596–2628.

(13) Lee, K.; Kim, S. W.; Toda, Y.; Matsuishi, S.; Hosono, H. Dicalcium nitride as a two-dimensional electride with an anionic electron layer. *Nature* **2013**, *494*, 336.

(14) Kitano, M.; Kanbara, S.; Inoue, Y.; Kuganathan, N.; Sushko, P. V.; Yokoyama, T.; Hara, M.; Hosono, H. Electride support boosts nitrogen dissociation over ruthenium catalyst and shifts the bottleneck in ammonia synthesis. *Nat. Commum.* **2015**, *6*, 6731.

(15) Lu, Y.; Li, J.; Tada, T.; Toda, Y.; Ueda, S.; Yokoyama, T.; Kitano, M.; Hosono, H. Water durable electride Y_5Si_3: Electronic structure and catalytic activity for ammonia synthesis. *J. Am. Chem. Soc.* **2016**, *138*, 3970–3973.

(16) Zhang, X.; Xiao, Z.; Lei, H.; Toda, Y.; Matsuishi, S.; Kamiya, T.; Ueda, S.; Hosono, H. Two-dimensional transition-metal electride Y_2C. *Chemistry of Materials* **2014**, *26*, 6638–6643.

(17) Zhang, Y.; Xiao, Z.; Kamiya, T.; Hosono, H. Electron confinement in channel spaces for one-dimensional electride. *J. Phys. Chem. Lett.* **2015**, *6*, 4966–4971.

(18) Walsh, A.; Scanlon, D. O. Electron excess in alkaline earth sub-nitrides: 2D electron gas or 3D electride? *J. Mater. Chem. C* **2013**, *1*, 3525–3528.

(19) Tada, T.; Takemoto, S.; Matsuishi, S.; Hosono, H. High-throughput ab initio screening for two-dimensional electride materials. *Inorg. Chem.* **2014**, *53*, 10347–10358.

(20) Inoshita, T.; Jeong, S.; Hamada, N.; Hosono, H. Exploration for two-dimensional electrides via database screening and ab initio calculation. *Phys. Rev. X* **2014**, *4*, 031023.

(21) Ming, W.; Yoon, M.; Du, M.-H.; Lee, K.; Kim, S. W. First-principles prediction of thermodynamically stable two-dimensional electrides. *J. Am. Chem. Soc.* **2016**, *138*, 15336–15344.

(22) Zhang, Y.; Wang, H.; Wang, Y.; Zhang, L.; Ma, Y. Computer-assisted inverse design of inorganic electrides. *Phys. Rev. X* **2017**, *7*, 011017.

(23) Park, J.; Lee, K.; Lee, S. Y.; Nandadasa, C. N.; Kim, S.; Lee, K. H.; Lee, Y. H.; Hosono, H.; Kim, S.-G.; Kim, S. W. Strong Localization of Anionic Electrons at Interlayer for Electrical and Magnetic Anisotropy in Two-Dimensional Y_2C Electride. *J. Am. Chem. Soc.* **2017**, *139*, 615–618.

(24) Hirayama, M.; Matsuishi, S.; Hosono, H.; Murakami, S. Topological Electride. *arXiv preprint arXiv:1801.03732* **2018**,

(25) Feng, C.; Shan, J.; Xu, A.; Xu, Y.; Zhang, M.; Lin, T. First-principle study of pressure-induced phase transitions and electronic properties of electride Y_2C. *Solid State Communications* **2017**, *266*, 34–38.

(26) Dale, S. G.; Otero-de-la Roza, A.; Johnson, E. R. Density-functional description of electrides. *Phys. Chem. Chem. Phys.* **2014**, *16*, 14584–14593.

(27) Dale, S. G.; Johnson, E. R. The explicit examination of the magnetic states of electrides. *Phys. Chem. Chem. Phys.* **2016**, *18*, 27326–27335.

(28) Li, S.; Ao, Z.; Zhu, J.; Ren, J.; Yi, J.; Wang, G.; Liu, W. Strain controlled ferromagnetic-antiferromagnetic transformation in Mn-doped silicene for information transformation devices. *J. Phys. Chem. Lett.* **2017**, *8*, 1484–1488.

(29) Blöchl, P. E. Projector augmented-wave method. *Phys. Rev. B* **1994**, *50*, 17953.

(30) others,, et al. QUANTUM ESPRESSO: A modular and open-source software project for quantum simulations of materials. *J. Phys. Condens. Mat.* **2009**, *21*, 395502.

(31) Marzari, N.; Vanderbilt, D.; De Vita, A.; Payne, M. C. Thermal contraction and disordering of the Al(110) surface. *Phys. Rev. Lett.* **1999**, *82*, 3296.

(32) Nielsen, O.; Martin, R. M. First-principles calculation of stress. *Phys. Rev. Lett.* **1983**, *50*, 697.

(33) Perdew, J.; Burke, K.; Ernzerhof, M. Generalized gradient approximation made simple. *Phys. Rev. Lett.* **1996**, *77*, 3865.

(34) Becke, A. D. Density functional calculations of molecular bond energies. *J. Chem. Phys.* **1986**, *84*, 4524–4529.

(35) Becke, A. D.; Johnson, E. R. Exchange-hole dipole moment and the dispersion interaction revisited. *J. Chem. Phys.* **2007**, *127*, 154108.

(36) Otero-de-la Roza, A.; Johnson, E. R. Van der Waals interactions in solids using the exchange-hole dipole moment model. *J. Chem. Phys.* **2012**, *136*, 174109.

(37) Otero-de-la Roza, A.; Johnson, E. R. A benchmark for non-covalent interactions in solids. *J. Chem. Phys.* **2012**, *137*, 054103.

(38) Johnson, E. R. In *Non-covalent interactions in quantum chemistry and physics*; Otero-de-la Roza, A., DiLabio, G. A., Eds.; Elsevier, 2017; Chapter 5, pp 215–248.

(39) Bader, R. F. A quantum theory of molecular structure and its applications. *Chem. Rev.* **1991**, *91*, 893–928.

(40) Pendás, A. M.; Blanco, M. A.; Costales, A.; Sánchez, P. M.; Luaña, V. Non-nuclear maxima of the electron density. *Phys. Rev. Lett.* **1999**, *83*, 1930.

(41) Johnson, E. R.; Otero-de-la Roza, A.; Dale, S. G. Extreme density-driven delocalization error for a model solvated-electron system. *J. Chem. Phys.* **2013**, *139*, 184116.

(42) Otero-de-la-Roza, A.; Blanco, M.; Pendás, A. M.; Luãna, V. Critic: A new program for the topological analysis of solid-state electron densities. *Comput. Phys. Commun.* **2009**, *180*, 157.

(43) Otero-de-la Roza, A.; Johnson, E. R.; Luaña, V. Critic2: A program for real-space analysis of quantum chemical interactions in solids. *Comp. Phys. Comm.* **2014**, 1007–1018.

(44) Yu, M.; Trinkle, D. R. Accurate and efficient algorithm for Bader charge integration. *J. Chem. Phys.* **2011**, *134*, 064111.

(45) Moeggenborg, K. J.; Papaioannou, J.; Dye, J. L. Powder conductivities of three electrides. *Chem. Mater.* **1991**, *3*, 514–520.

(46) Inoshita, T.; Hamada, N.; Hosono, H. Ferromagnetic instability of interlayer floating electrons in the quasi-two-dimensional electride Y_2C. *Phys. Rev. B* **2015**, *92*, 201109.

(47) Pickard, C. J.; Needs, R. Predicted pressure-induced s-band ferromagnetism in alkali metals. *Phys. Rev. Lett.* **2011**, *107*, 087201.

(48) Dale, S. G.; Johnson, E. R. Thermodynamic cycles of the alkali metal-ligand complexes central to electride formation. *Phys. Chem. Chem. Phys.* **2017**, *19*, 12816–12825.

Graphical TOC Entry